Available online at www.sciencedirect.com

SciVerse ScienceDirect

Ceramics International 38 (2012) 6541–6548

CERAMICS INTERNATIONAL

www.elsevier.com/locate/ceramint

C/SiC–ZrB_2–ZrC composites fabricated by reactive melt infiltration with $ZrSi_2$ alloy

Huilong Pi, Shangwu Fan, Yiguang Wang*

Science and Technology on Thermostructure Composite Materials Laboratory, Northwestern Polytechnical University, Xi'an 710072, Shaanxi, PR China

Received 6 May 2012; received in revised form 11 May 2012; accepted 12 May 2012
Available online 30 May 2012

Abstract

C/SiC–ZrB_2–ZrC composites were prepared by reactive melt infiltration (RMI) combined with vacuum pressure impregnation (VPI) method. B_4C–C was first introduced into C/SiC composites with a porosity of about 30% by impregnating the mixture of B_4C and phenol formaldehyde resin, followed by pyrolysis at 900 °C. The molten $ZrSi_2$ alloy was then infiltrated into the porous C/SiC–B_4C–C to obtain C/SiC–ZrB_2–ZrC composites. The flexural strength was tested. The ablation behavior was investigated under an oxyacetylene torch flame. It has been found that the C/SiC–ZrB_2–ZrC showed a high flexural strength and an excellent ablation resistance. The reactions between $ZrSi_2$ alloy and B_4C–C were studied, and a model based on these reactions was built up to describe the formation mechanism of the matrix.

Keywords: Ceramic matrix composites (CMCs); Rective melt infiltration; Ablation; Foramtion mechanism

1. Introduction

Hypersonic vehicles that will fly at hypersonic speed require the materials capable of prolonged operation in oxidizing atmosphere above 2000 °C [1–4]. The high-temperature materials like C/C, C/SiC, and SiC/SiC cannot withstand ablation environment at such high temperatures [3–9]. Ultra high temperature ceramics (UHTCs) may satisfy the temperature requirements for hypersonic vehicles due to their extremely high melting point higher than 3000 °C [10,11]. ZrB_2 and ZrC are considered the most promising materials in ultra high-temperature ceramic family due to their high melting points (3250 °C and 3540 °C, respectively) and low densities (6.1 g/cm^3 and 6.7 g/cm^3, respectively). Adding appropriate amounts of SiC into ZrB_2, its ablation resistance and oxidation resistance will be greatly enhanced [11]. However, monolithic UHTCs are very brittle and display poor thermal shock resistance [12,13]. Continuous carbon fibers reinforced ultra-high temperature ceramic composites (C_f/UHTC) would gain excellent properties owing to the combination of an ultrahigh temperature durable ceramic matrix and mechanically tough reinforcements [12,13].

In the past years, a large number of researches have been carried out on the preparation of C/UHTC by adding UHTC compositions into C/C or C/SiC composites. Li et al. introduced ZrB_2/ZrC into C/SiC by using powder infiltration [13,14]. Wang et al. fabricated 2D C/ZrB_2–SiC composites by slurry pasting PCS/ZrB_2 combined with CVI method [15]. Tong et al. prepared ZrC/C composites by using hot-pressing method [16]. Dong et al. fabricated C_f/ZrC–SiC composites by polymer infiltration and pyrolysis combined with ZrC precursor impregnation [17]. However, the increase in the ablation resistance of these composites is so limited because the refractory carbide/boride content in these C/UHTCs is low. Recently, RMI technology was used to fabricate C/UHTC in order to introduce more refractory carbide into the composites [12,18]. The results of these ablation tests showed that those composites had excellent ablation resistance.

Previous study indicated that the addition of ZrC to SiC–ZrB_2 to form a ternary ceramics of SiC–ZrB_2–ZrC can obtain a superior resistance to ablation at high

*Corresponding author. Tel.: +86 29 88494914; fax: +86 29 88494620.
E-mail address: wangyiguang@nwpu.edu.cn (Y. Wang).

0272-8842/$36.00 © 2012 Elsevier Ltd and Techna Group S.r.l. All rights reserved.
http://dx.doi.org/10.1016/j.ceramint.2012.05.035

temperatures [19]. The ternary ceramic matrix of SiC–ZrB_2–ZrC in carbon fiber reinforced composites is assumed to have a better ablation resistance than the binary ceramic matrix of SiC–ZrB_2 or SiC–ZrC in the composites. As aforementioned, the introduction of ZrB_2–ZrC into matrix by slurry paste or impregnation was so limited that the increase in ablation resistance was not obvious. The introduction of ZrB_2 into the matrix by RMI has been rarely reported so far. In this paper, we reported a combination process of vacuum pressure impregnation (VPI) and RMI to fabricate the ternary matrix of SiC–ZrB_2–ZrC in the composites. The formation mechanism of the ternary matrix was studied and a model based on these analysis results was built up to describe the reaction mechanism. The ablation properties of the as-fabricated composites were also evaluated under an oxyacetylene torch flame.

2. Experimental procedure

2.1. Material preparation

Fig. 1 shows the fabrication process of the C/SiC–ZrB_2–ZrC composites. The T-300^{TM} plain woven carbon cloth (fiber volume fraction ~40%, Toray, Japan) was cut into 100 mm × 100 mm pieces. These fiber cloths were stacked along cloth plain to form a porous preform. A thin pyrocarbon layer was then deposited on the fiber to obtain a weak interphase. 2D C/SiC composites with a porosity of 30% were fabricated by chemical infiltration (CVI) method at 1000 °C using methyltrichlorosilane (MTS, CH_3SiCl_3) as precursor [20]. The B_4C-phenol formaldehyde resin (PF) slurry was prepared as follows: first, the PF (PF 2313, 96.5% purity, Xian resin factory, Xian, China) was dissolved in a mixed acetone/ethanol solvent, and then the B_4C (Feret diameter 0.5 μm, 99% purity, Lihua Gaoke Chemical Company, Beijing, China) was added into the PF solution. This slurry was then ball-milled for 36 h using ZrO_2 balls. The 2D C/SiC composites were impregnated by this slurry, followed by pyrolysis at 900 °C. The process of impregnation and pyrolysis was repeated 3,4 times to introduce B_4C–C into C/SiC composites. The $ZrSi_2$ alloy powder (99.5% purity, Hai Chem. Co. LTD., Beijing, china) was molten in a vacuum at 1800 °C. The molten $ZrSi_2$ alloy was infiltrated into the C/SiC–B_4C–C preform by capillary forces along the pores between carbon fiber tows, where it reacted with the B_4C–C to form ZrB_2–ZrC–SiC matrix. Finally, a SiC coating was deposited on the composites by chemical vapor deposition (CVD) method.

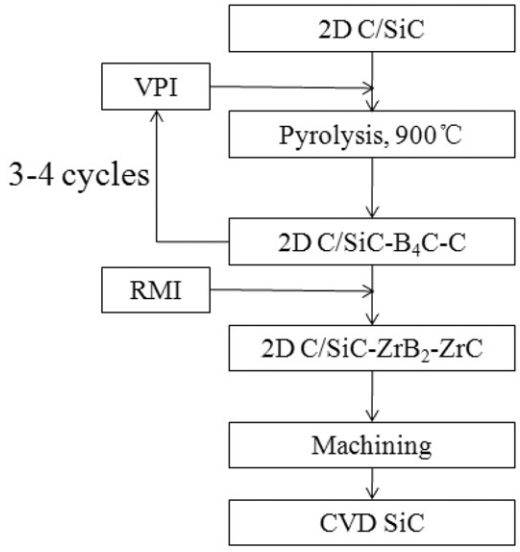

Fig. 1. Fabrication process for the C/SiC–ZrB_2–ZrC composites.

2.2. Tests and characterization

The flexural strength was measured using a three-point bending test (SANS CMT 4304, Sans Testing Machine, Shen Zhen, China) with a span of 30 mm. At least three samples with a dimension of 40 mm × 5 mm × 3 mm were used for the test. The loading rate was 0.5 mm/min, and the loading direction was perpendicular to the carbon cloth plain. The force-displacement curves were recorded by computer. The ablation tests were carried out in a vertically jetted flowing oxyacetylene torch environment. The exposure time under the torch flame was 20 s. The distance between the nozzle tip of the oxyacetylene gun and the center of the specimen surface was 10 mm. The inner diameter of the nozzle tip was 2 mm. The pressures of oxygen and acetylene were 0.4 MPa and 0.095 MPa, respectively. The flowing rate was 0.42 L/s for oxygen and 0.31 L/s for acetylene. The detail test process can be found in reference [21–23]. At least three samples with a dimension of Φ30 mm × 5 mm were used in the test. The phase composition of the composite was investigated by X-ray diffraction analysis (XRD, D/max-2400, Rigaku, Japan) with Cu K_α radiation. Data were digitally recorded in a continuous scan mode in the angle (2θ) range of 10–80° with a scanning rate of 0.12 °s. The microstructures of the specimens were observed by scanning electron microscope (SEM, JEOL 6700F, Tokyo, Japan) and the elemental analysis was conducted by energy dispersive spectroscopy (EDS). The density of the samples was measured by the Archimedes method with distilled water.

3. Results and discussion

3.1. Characterization of C/SiC–ZrB_2–SiC composites

The original 2D C/SiC composites, which are performs with a porosity of around 30 vol%, have many big holes between fiber bundles (Fig. 2a). These big holes were then filled by B_4C–C by repeating the process of impregnating B_4C–PF slurry, followed by pyrolysis at 900 °C for several times. As shown in Fig. 2b, the pores were well occupied by the mixture of B_4C and carbon. The enlarged image (Fig. 2c) clearly showed that the clusters of B_4C powders

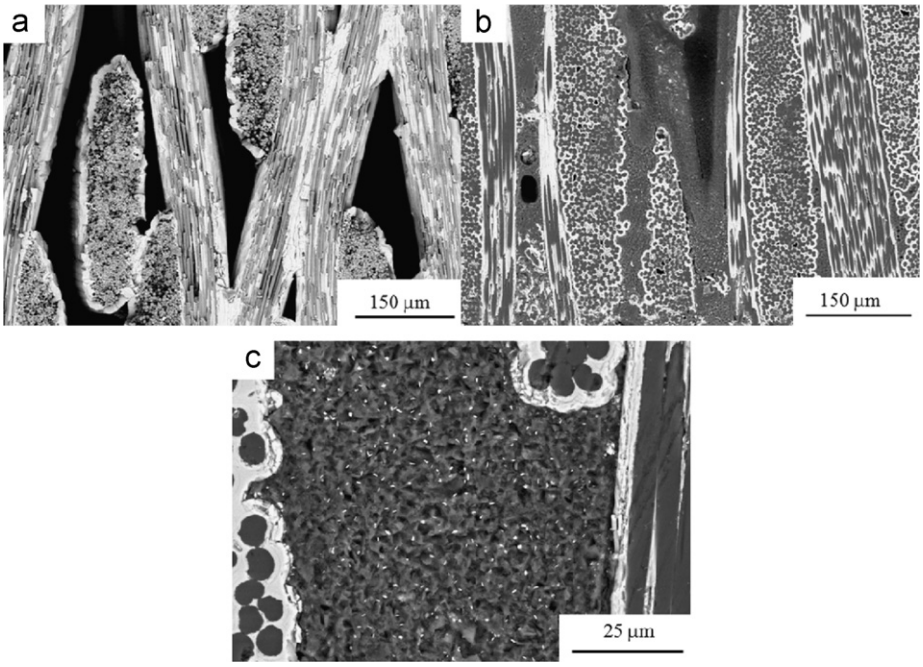

Fig. 2. Back-scattered electron images for cross-sections of the different composites (a) The cross-section of the porous C/SiC preform; (b) the polished cross-section of the C/SiC–B_4C–C; (c) the B_4C–C between fiber bundles.

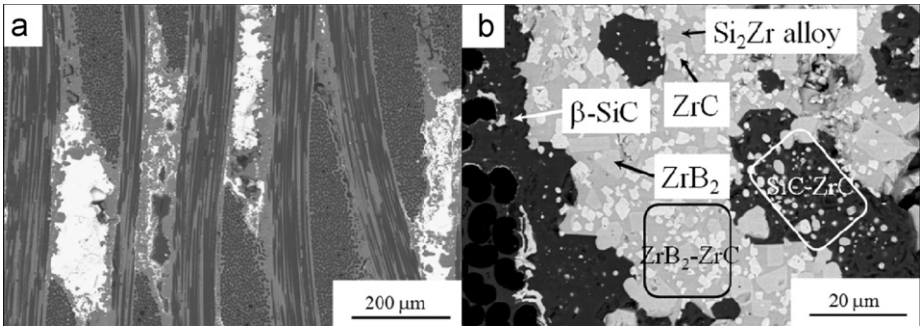

Fig. 3. Back-scattered electron images for polished cross-sections of C/SiC–ZrB_2–ZrC composites (a) the cross-section of C/SiC–ZrB_2–ZrC; (b) the distribution of SiC–ZrB_2–ZrC matrix.

with the surrounding pyrolytic carbon were distributed evenly between the fiber bundles.

After infiltrating the $ZrSi_2$ into the porous C/SiC–B_4C–C at 1800 °C, the C/SiC–ZrB_2–ZrC composites were obtained. Fig. 3a shows a typical cross-section of C/SiC–ZrB_2–ZrC composites. It is seen that the inter-bundle are filled with the generated white matrix, which is the in-situ formed SiC–ZrB_2–ZrC. The formed matrix is dense except a few of microscopic voids in it. The detail microstructure of the C/SiC–ZrB_2–ZrC composites is shown in Fig. 3b. As can be seen, a CVI SiC layer is around the carbon fiber bundles. This CVI SiC layer will protect carbon fibers and PyC interface from destroying by molten $ZrSi_2$ alloy during RMI process. Far from CVI SiC layer, the inter-bundle areas are filled with the formed ZrC–ZrB_2–SiC during the RMI processing. Fig. 3b further indicates that there are two regions in the generated ZrC–ZrB_2–SiC matrix: ZrC–SiC region lack of ZrB_2 and ZrB_2–ZrC region in which no SiC could be found except a small friction of $ZrSi_2$ residual.

Fig. 4 shows the XRD pattern of the C/SiC–ZrB_2–SiC composites. It indicates that ZrB_2, ZrC, SiC, and C are the main phases. A small amount of residual $ZrSi_2$ alloy is also detected by XRD, coinciding with the microscopic observation. The results indicate that most of the infiltrated $ZrSi_2$ alloy has reacted with B_4C–C to form ZrB_2–ZrC–SiC matrix.

3.2. The formation mechanism of C/SiC–ZrB_2–ZrC composites

The formation of SiC–ZrB_2–SiC matrix can be discussed based on the Zr–Si–C phase diagram and the $ZrSi_2$–B_4C (Fig. 5a) phase diagram that was calculated by using FactSage programs (Thermfact/CRCT & GTT-Technologies, Canada and Germany). As indicated in Fig. 2c, the aggregated B_4C powders were surrounded by pyrolytic carbon. The schematic

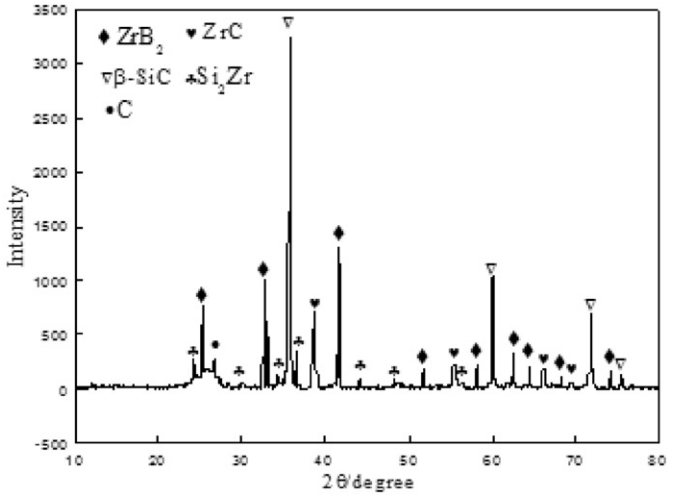

Fig. 4. XRD pattern of C/SiC–ZrB_2–ZrC composites fabricated at 1800 °C for 30 min.

drawing of such a structure is shown in Fig. 5b. During the infiltration of molten $ZrSi_2$ into the C/SiC–B_4C–C preform at 1800 °C, $ZrSi_2$ alloy will first react with the surrounding pyrolytic carbon. Our previous study indicated that $ZrSi_2$ reacted with C to form the mixture of SiC and ZrC according to Zr–Si–C ternary phase diagram [18]. The produced SiC is more than ZrC according to lever principle. When the $ZrSi_2$ alloy meets the B_4C clusters, it will react with B_4C. At the present condition, the $ZrSi_2$ melt is superfluous compared with the content of B_4C due to the continuous support of $ZrSi_2$ melt from the reservoir. According to the $ZrSi_2$–B_4C phase diagram (Fig. 5a), the reaction products of B_4C and excess $ZrSi_2$ alloy melt at 1800 °C should be ZrB_2, ZrC, and some residual $ZrSi_2$. The schematic reaction process is shown in Fig. 5b. According to Fig. 5b, two regions are formed after reactions. One is ZrC–SiC region from the reaction of $ZrSi_2$ with pyrolytic carbon; the other is ZrB_2–ZrC region from the reaction of $ZrSi_2$ with B_4C. The results are well in agreement

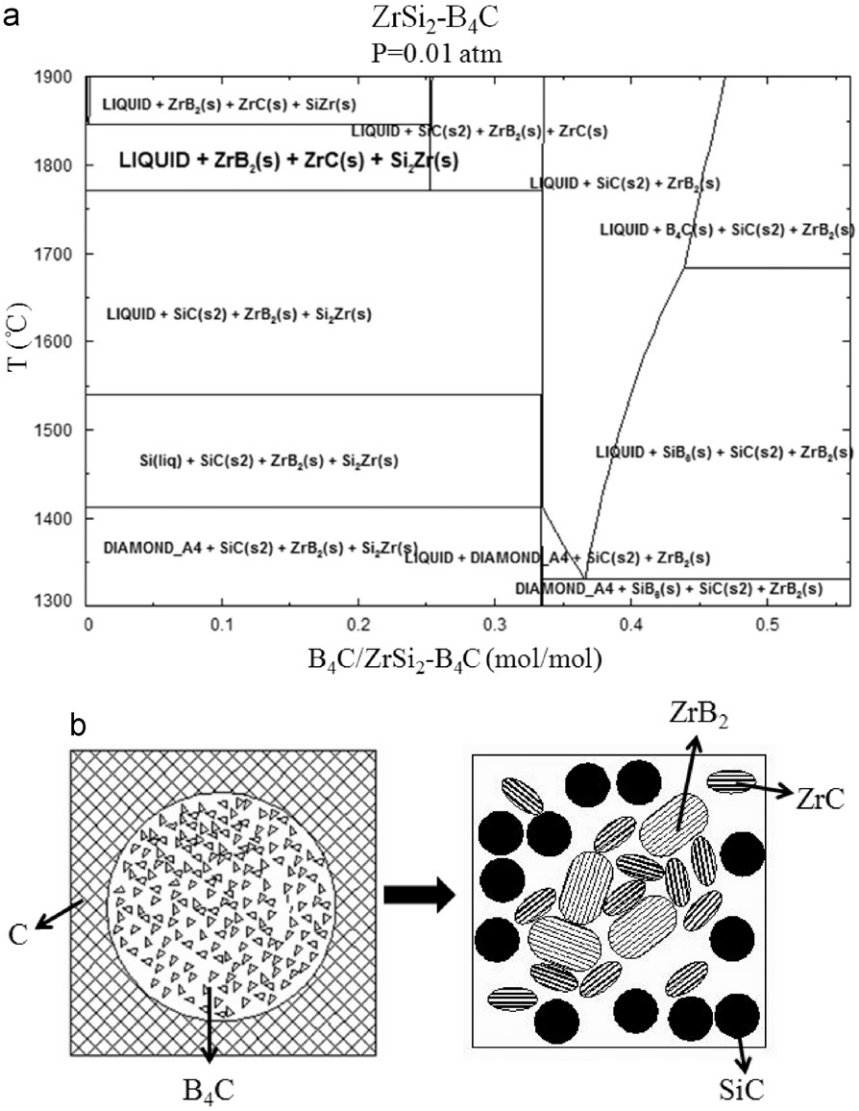

Fig. 5. (a) the calculated $ZrSi_2$–B_4C phase diagram (b) the model of the reaction between $ZrSi_2$ alloy and B_4C–C.

with the distribution of ZrB_2, ZrC and SiC in the matrix showed in Fig. 3b.

3.3. Mechanical properties of C/SiC–ZrB_2–ZrC composites

The flexural load-displacement curve of C/SiC–ZrB_2–ZrC composites is shown in Fig. 6a. The flexural strength of C/SiC–ZrB_2–ZrC is calculated to be 380 ± 9 MPa. The C/SiC–ZrB_2–ZrC composites show pseudoplastic behavior due to the crack deflection (Fig. 6b), interfacial debonding and fiber pull-out (Fig. 6c). The bending strengths of 2D C/SiC [8], 2D C/ZrB_2–SiC [15], 2D C/SiC–ZrB_2–TaC [21], and C/SiC–ZrB_2–ZrC are compared in Table 1. It is seen that the strength of C/SiC–ZrB_2–ZrC are greatly enhanced. The high bending strength of the C/SiC–ZrB_2–ZrC composites result from the well protected fiber tows (Fig. 6) and the in-situ formed ZrB_2–ZrC–SiC matrix that has high interface bonding strength, leading to the retard of the crack propagation [10].

3.4. Ablation behavior of C/SiC–ZrB_2–ZrC composites

The macrographic pictures of C/SiC–ZrB_2–ZrC before and after ablation test are shown in Fig. 7a and Fig. 7b, respectively. A white, loose ablation layer can be found on the ablated surface of C/SiC–ZrB_2–ZrC composites. The most serious ablation happens in the center of the flame. The dimensional change of the samples before and after ablation test was measured to obtain the linear ablation rate. The linear ablation rate of the C/SiC–ZrB_2–ZrC is listed in Table 1. As a comparison, 2D C/SiC, 2D C/ZrB_2–SiC [15], and 2D C/SiC–ZrB_2–TaC [21] are also shown in Table 1. Among these composites, the C/SiC–ZrB_2–ZrC exhibits the best ablation resistance in the oxyacetylene torch environments. XRD pattern of the surface on the ablated samples (Fig. 7c) indicates that the white layer consists of a mixture of ZrO_2 and a little of SiO_2. From the microstructure and EDS (Fig. 8d–f) analysis of ablation surface, it can be seen that ZrO_2 and silica melt are formed during the ablation process. ZrB_2 and ZrC cannot be identified by XRD because their contents on the surface are little after ablation test. The following reactions would happen during the ablation process [17–19]:

$$2ZrB_2\ (s) + 5O_2 \times (g) = 2ZrO_2 \times (s,l) + 2B_2O_3 \times (g) \quad (1)$$

$$2ZrC \times (s) + 3O_2 \times (g) = 2ZrO_2 \times (s,l) + 2CO \times (g) \quad (2)$$

$$2SiC \times (s) + 3O_2 \times (g) = 2SiO_2 \times (l) + 2CO \times (g) \quad (3)$$

$$SiC \times (s) + O_2(g) = SiO(g) + CO(g) \quad (4)$$

Table 1
The flexural strength and linear ablation rates of 2D C/SiC, 2D C/SiC–ZrB_2, 2D C/SiC–ZrB_2–TaC and C/SiC–ZrB_2–ZrC.

Sample	Flexural strength (MPa)	Line-ablation rate (mm/s)	Density (g/cm^3)	Open porosity (%)
2D C/SiC–ZrB_2–ZrC	380 ± 9	0.002 ± 0.001	2.23	10
2D C/SiC	350 ± 15 [8]	0.042 ± 0.012	2.07	10
2D C/ZrB_2–SiC [15]	237 ± 30	0.066	2.10	–
2D C/SiC–ZrB_2–TaC[21]	225 ± 15	0.026	2.35	11.5

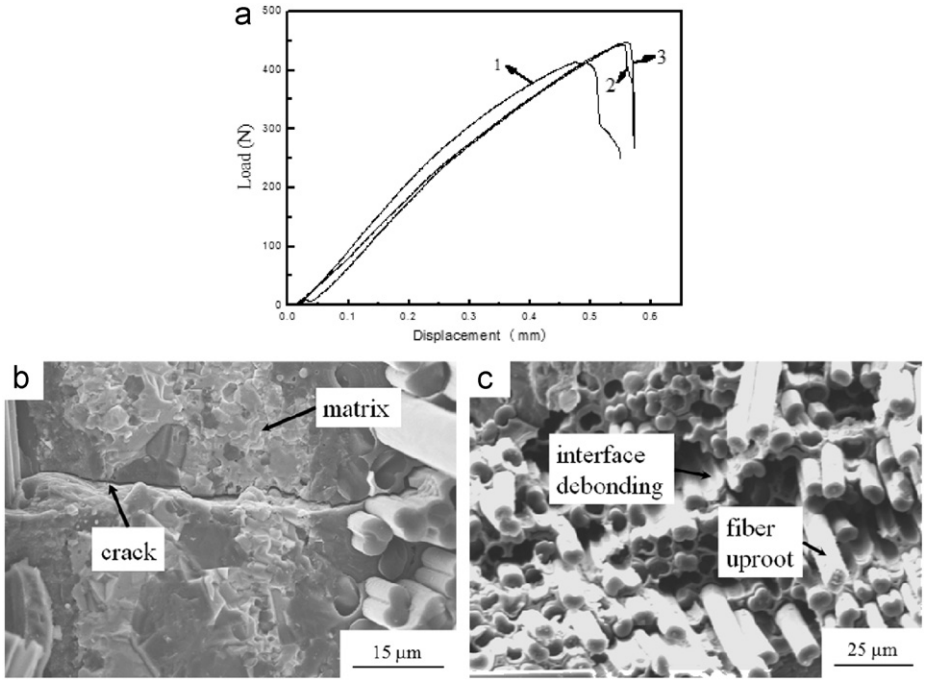

Fig. 6. (a) Force-displacement curves of C/SiC–ZrB_2–ZrC composites, (b) the fracture surface of the composites indicating crack deflection, (c) and the fracture surface of the composites indicating the interface debonding and fiber uproot.

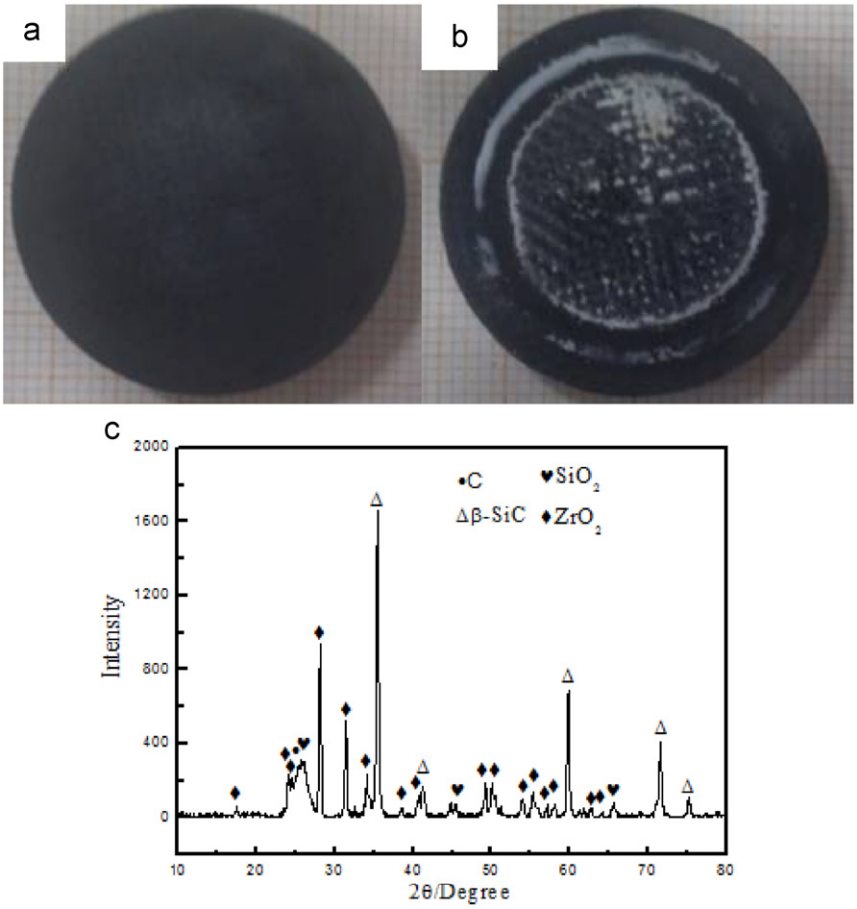

Fig. 7. Macrographic pictures of C/SiC–ZrB_2–ZrC before (a) and after ablation (b), and XRD pattern of the ablation surface (c).

Fig. 7 indicates that there are three typical ablation regions on the surface of C/SiC–ZrB_2–ZrC composites: the ablation fringe, ablation center, and a region between them. The temperature at the center of the ablated sample is about 3000 °C, while the temperatures in the ablation fringe region are less than 1800 °C [22,23]. Fig. 8c shows the morphology of the surface at the ablation fringe, in which the materials are slightly oxidized and no obvious mass loss. At the center of the ablated flame (Fig. 8a), the temperature is about 3000 °C, which results in the quick loss of SiO_2 and B_2O_3. At such high temperatures, SiC are actively oxidized and B_2O_3 almost evaporates out. ZrO_2, which has very high melting point (2850 °C) and low vapor pressure, will mix with SiO_2 to form Zr–Si–O glass (Fig. 8d). The Zr–Si–O glass has higher melting point than SiO_2, and is difficult to be blown away by the gas flow. Therefore, the Zr–Si–O glass covered on the fibers can prevent the fibers from being oxidized (Fig. 8b). However, Zr–Si–O glass has not been formed a continuous layer and its protection for composites is limited. Between the center and the ablation fringe, the temperature is in the range of 1700–2700 °C, B_2O_3 also evaporates very fast and the ZrO_2 is porous skeleton. Fig. 8c shows that the porous ZrO_2 skeleton will be filled with melt SiO_2 glass to form a dense ZrO_2–SiO_2 layer. The dense ZrO_2–SiO_2 layer can bear the mechanical erosion of oxyacetylene torch flame and protect the composites. The good ablation resistance of the C/SiC–ZrB_2–ZrC composites results from the protection of these oxides.

4. Conclusion

C/SiC–ZrB_2–ZrC composites were fabricated by RMI process combine with VPI method. B_4C–C was introduced into 2D C/SiC by repeating the process of impregnation of the B_4C–PF slurry, followed by pyrolysis at 900 °C. Then the molten $ZrSi_2$ alloy was infiltrated into the C/SiC–B_4–C perform to in-situ form ZrB_2–ZrC–SiC matrix. The formed ZrB_2–ZrC–SiC matrix was divided into two regions of SiC–ZrC and ZrB_2–ZrC based on the distribution of ZrB_2, ZrC and SiC. The reaction mechanisms were discussed based on the Zr–Si–C ternary phase diagram and $ZrSi_2$–B_4C phase diagram. The C/SiC–ZrB_2–SiC composites showed a high bending strength due to the in-situ formed ZrB_2–ZrC–SiC. The linear ablation rate of the C/SiC–ZrB_2–ZrC composites is 0.002 mm/s. The ablation resistance of the C/SiC–ZrB_2–ZrC composites obviously increased due to the formation of Zr–Si–O glass and ZrO_2–SiO_2 continuous layer to protect fibers and matrix from ablation.

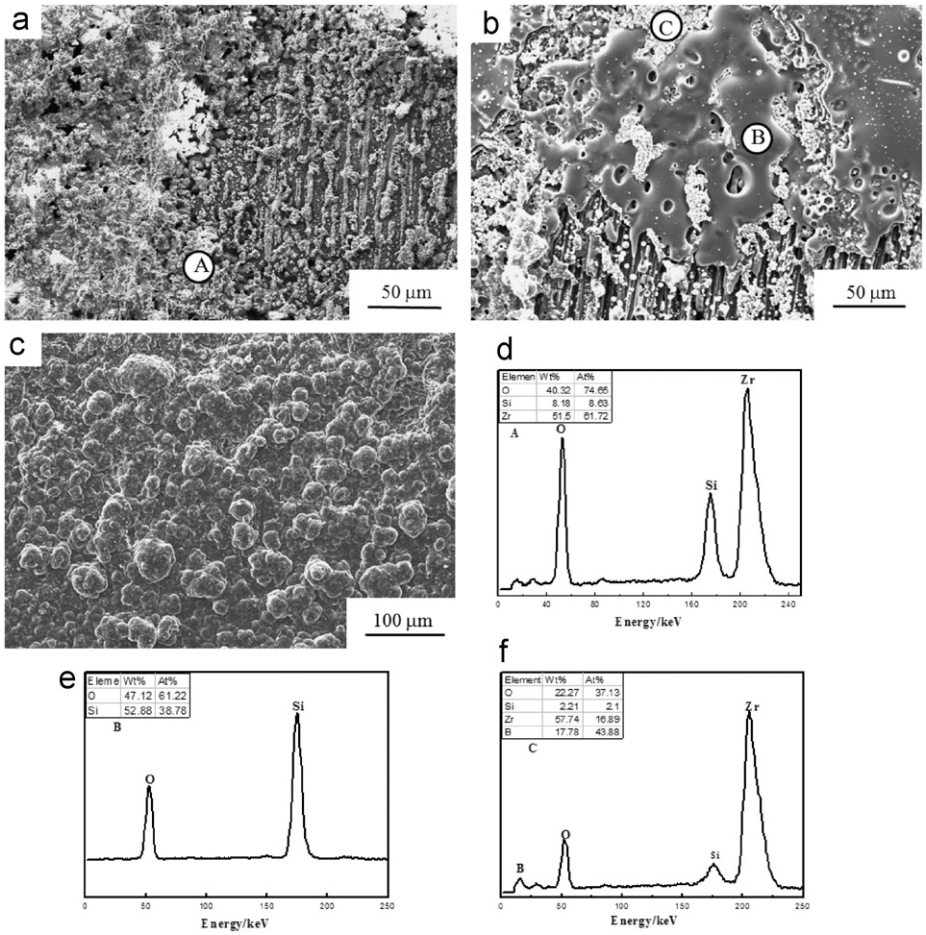

Fig. 8. Morphologies of the ablated surface in oxyacetylene flame: (a) the center region; (b) the region near to the ablation center; (c) the low-temperature region and the EDS analysis of different spots (d)–(f).

Acknowledgements

This work is financially supported by the Chinese Natural Science Foundation (Grant no #51172181) and "111" project (B08040).

References

[1] S. Schmidt, S. Beyer, H. Knabe, H. Immich, R. Meistring, A. Gessler, Advanced ceramic matrix composite materials for current and future pro-pulsion technology applications, Acta Astronautica 55 (2004) 409–420.

[2] R.R. Naslain, Processing of non-oxide ceramic matrix composites: an overview, Advanced Science and Technology 50 (2006) 64–74.

[3] K. Upadhya, J.M. Yang, W.P. Hoffman, Materials for ultrahigh temperature application, Journal of the American Ceramic Society 76 (1997) 51–56.

[4] T.H. Squire, J. Marschall, Material property requirements for analysis and design of UHTC composites in hypersonic applications, Journal of the European Ceramic Society 30 (2010) 2239–2251.

[5] T.M. Besmann, B.W. Sheldon, R.A. Lowden, D.P. Stinton, Vapor phase fabrication and properties of continuous filament ceramic composites, Science 253 (1991) 1104–1109.

[6] T. Ishikawa, S. Kajii, K. Matsunaga, T. Hogami, Y. Kohtoku, T. Nagasawa, A tough, thermally conductive silicon carbide composite with high strength up to 1600 °C in air, Science 282 (1998) 1295–1297.

[7] D.R. Lide, Handbook of Chemistry and Physics, 79th ed., CRC Press, Boca Raton, FL, 1998.

[8] F. Lamouroux, G. Gamus, Oxidation effects on the mechanical properties of 2D woven C/SiC composites, Journal of the European Ceramic Society 14 (1994) 177–188.

[9] F. Christin, Design, fabrication, and application of thermostructural composites (TSC) like C/C, C/SiC, and SiC/SiC composites, Advanced Engineering Materials 4 (2002) 903–912.

[10] R. Licheri, R. Orru, C. Musa, G. Cao, Combination of SHS and SPS techniques for fabrication of fully dense ZrB_2–ZrC–SiC composites, Materials Letters 62 (2008) 432–435.

[11] W.W. Wu, G.J. Zhang, Y.M. Kan, P.L. Wang, Reaction hot pressing of ZrB_2–SiC–ZrC ultra high-temperature ceramics at 1800 °C, Journal of the American Ceramic Society 89 (2006) 2967–2969.

[12] L. Zou, N. Wali, J.M. Yang, Microstructural characterization of a C_f/ZrC composite manufactured by reactive melt infiltration, Journal of Applied Ceramic Technology 8 (2011) 329–341.

[13] H.P. Li, L.T. Zhang, L.F. Cheng, Y.G. Wang, Ablation resistance of different coating structures for C/ZrB_2–SiC composites under oxyacetylene torch flame, Journal of Applied Ceramic Technology 6 (2009) 145–150.

[14] H.P. Li, L.T. Zhang, L.F. Cheng, Y.G. Wang, Fabrication of 2D C/ZrC–SiC composite and its structural evolution under high-temperature treatment up to 1800 °C, Ceramics International 35 (2009) 2831–2836.

[15] Y.G. Wang, W. Liu, L.F. Cheng, L.T. Zhang, Preparation and properties of 2D C/ZrB_2–SiC ultra high temperature ceramic composites, Journal of Applied Ceramic Technology 524 (2009) 129–133.

[16] Q.F. Tong, J.L. Shi, Y.Z. Song, Q.G. Guo, L. Liu, Resistance to ablation of pitch-derived ZrC/C composites, Carbon 42 (2004) 2495–2500.

[17] Q.Q. Li, S.M. Dong, Z. Wang, P. He, H.J. Zhou, J.S. Yang, B. Wu, J.B. Hu, Fabrication and properties of 3D C/SiC–ZrC composites using ZrC precursor and polycarbosilane, Journal of the American Ceramic Society 95 (2012) 1216–1219.

[18] Y.G. Wang, X.J. Zhu, L.T. Zhang, L.F. Cheng, Reaction kinetics and ablation properties of C/C–ZrC composites fabricated by reactive melt infiltration, Ceramics International 37 (2011) 1277–1283.

[19] Q. Qu, J.C. Han, W.B. Han, X.H. Zhang, C.Q. Hong, In situ synthesis mechanism and characterization of ZrB_2–ZrC–SiC ultra high-temperature ceramics, Journal of Materials Chemistry and Physics 110 (2008) 216–221.

[20] Z.X. Meng, L.F. Cheng, L.T. Zhang, Y.D. Xu, X.F. Han, Microstructures, strength and toughness of 2D Cf/SiC composites by chemical vapor infiltration, Journal of Inorganic Materials 24 (2009) 939–942.

[21] L.L. Li, Y.G. Wang, L.F. Cheng, L.T. Zhang, Preparation and properties of 2D C/SiC–ZrB_2–TaC composites, Ceramics International 34 (2011) 891–896.

[22] Y.G. Wang, X.J. Zhu, L.T. Zhang, F.L. Cheng, C/C–SiC–ZrC composites fabricated by reactive melt infiltration with $Si_{0.87}Zr_{0.13}$ alloy, Ceramics International 38 (2012) 4337–4343.

[23] Y.G. Wang, Y.D. Xu, Y. Wang, L.F. Cheng, L.T. Zhang, Effects of TaC addition on the ablation resistance of C/SiC, Materials Letters 64 (2010) 2068–2071.